Oxygen-ordering superstructures in underdoped $YBa_2Cu_3O_{6+x}$ studied by hard x-ray diffraction

M. v. Zimmermann and J. R. Schneider
Hamburger Synchrotronstrahlungslabor HASYLAB at Deutsches Elektronen-Synchrotron DESY, Notkestrasse 85, D-22603 Hamburg, Germany

T. Frello, N. H. Andersen, J. Madsen, M. Käll, and H. F. Poulsen
Materials Research Department, Risø National Laboratory, DK-4000 Roskilde, Denmark

R. Liang, P. Dosanjh, and W. N. Hardy
Department of Physics, The University of British Columbia, Vancouver, British Columbia, Canada V6T 1Z1
(Received 9 January 2003; revised manuscript received 2 June 2003; published 18 September 2003)

High-energy x-ray diffraction is used to investigate the bulk oxygen-ordering properties of $YBa_2Cu_3O_{6+x}$. Four different superstructures of Cu-O chains aligned along the *b* axis and ordered with periodicity ma, along the *a* axis have been observed. For $x<0.62$, the only observed superstructure is ortho-II with $m=2$. At room temperature, we find ortho-III ($m=3$) for $0.72\leqslant x\leqslant 0.82$, ortho-V ($m=5$) in a mixed state with ortho-II at $x=0.62$, and ortho-VIII ($m=8$) at $x=0.67$. Ortho-II is a three-dimensional ordered structural phase, the remaining ones are essentially two-dimensional. None of the superstructures develops long-range ordering. The temperature dependence of the observed superstructure ordering is investigated explicitly and a structural phase diagram is presented.

DOI: 10.1103/PhysRevB.68.104515 PACS number(s): 61.10.−i, 68.35.Rh, 74.72.Bk

I. INTRODUCTION

While the Cu-O chain structure containing variable amount of oxygen, *x*,[1] gave rise to some confusion when superconductivity was discovered in $YBa_2Cu_3O_{6+x}$ (YBCO), it is nowadays well established that the chains act as the charge reservoir, creating the holes in the CuO_2 planes. Sufficient charge transfer for superconductivity occurs when the Cu-O chains become sufficiently long and form the orthorhombic phase by aligning along the crystallographic *b* direction for $x\geqslant 0.35$.[2–4] The importance of oxygen ordering for the superconducting properties has been verified directly from experimental studies where crystals are quenched from the tetragonal disordered into the orthorhombic ordered phase. Here it is found that T_c of quenched YBCO is reduced compared to the equilibrium value and increases with time when the sample is annealed at room temperature.[5–8] Equally, it has been observed that the oxygen ordering of quenched YBCO crystals increases with time.[9,10] For well-equilibrated samples, T_c varies within the orthorhombic phase from around 35 K at $x=0.35$ to $T_c=93$ K for the optimally doped material ($x=0.93$) and exhibits a plateau at 60 K around $x=0.5$,[11] a variation that has been shown to comply with the generic relation between hole doping and T_c in the high-T_c materials.[12]

When the Cu-O chains align along the *b* axis in the basic ortho-I structure, the oxygen occupies the so-called O(1) site, whereas the sites on the *a* axis [O(5)] are essentially empty. Ortho-I is a three-dimensional (3D) long-range-ordered structure, but in commonly prepared crystals true long-range order is prevented by the formation of twin domains with domain size ranging from a few hundred Angstrøm to macroscopic size. Clearly, there is disorder in the ortho-I chain structure for compositions $x<1.0$. Therefore, in thermodynamic equilibrium ordered superstructures must be formed for $T\rightarrow 0$ inside the ortho-I twin domains.[13]

Despite all the experimental and theoretical studies performed, the microscopic understanding of the relation between oxygen composition and ordering on one hand and the magnetic, electronic/superconducting properties on the other is still not satisfactory. Among the reasons for this are the slow oxygen-ordering kinetics at room temperature and the sensitivity to crystal defects, making the availability of high-quality single crystals and proper thermal sample treatment particularly important. Thus, with emphasis on these problems a thorough study of the oxygen-ordering properties as function of *x* is mandatory for further development of understanding. This has become even more important since it has recently been suggested that the CuO_x chains are correlated with instabilities in the CuO_2 planes, which can be thought of as stripelike patterns using the oxygen ordering as a template.[14]

Electron microscopy techniques have contributed significantly to establish the superstructures of YBCO.[17–20] Superstructure reflections with periodicity ma along the *a* axis are found at modulation scattering vectors: $\mathbf{Q}=(nh_m,0,0)$, where $h_m=1/m$, and $n<m$ are integers, and the coordinates refer to the reciprocal lattice vectors. Superstructures with $m=2$, 3, 4, 5, and 8 have been observed experimentally and are named ortho-II, ortho-III, ortho-IV, ortho-V, and ortho-VIII, respectively. In real space these superstructures are characterized by different sequences of full Cu-O and empty Cu chains. The need for confirmation by bulk structural techniques is generally recognized, because electron-beam heating of thin crystals may change the mobile oxygen content *x* and generate transient nonequilibrium surface structures. Also, it is difficult to obtain quantitative details about the atomic positions, finite-size ordering properties, and their temperature dependence by these techniques. Analysis of structure factors obtained from a combination of neutron- and x-ray-diffraction data has unequivocally shown that the ortho-II and ortho-III superstructures result from oxygen or-

dering in Cu-O chains,[21–28] but the relaxation of cations associated with the oxygen chain ordering contributes significantly to the superstructure intensities. In particular, the barium displacement has a strong influence on the x-ray-diffraction intensity, which is displaced by about 0.04 Å along the *x* direction with respect to the average structure. The Cu(2) site and O(4) are also significantly displaced along the *z* direction, while no displacements along the *y* direction have been found.[28,29] These displacements show only minor variation with oxygen composition.[25,29] Also, in the ortho-II phase there was found no significant change in the displacements as function of temperature.[30] Superstructures with unit cells $2\sqrt{2}a\times 2\sqrt{2}a\times c$ (Refs. 18,31,32) and $\sqrt{2}a\times 2\sqrt{2}a\times c$,[21] the so-called herringbone type, have been reported. Although this type of superstructures have been identified in $NdBa_2Cu_3O_{6+x}$,[33] they are, as we shall discuss in Sec. IV, most likely not from oxygen ordering in YBCO.

In the present paper, we report on experimental studies of the oxygen ordering in YBCO covering the oxygen compositions $0.35\leqslant x\leqslant 0.87$ and temperatures up to 250 °C, by diffraction of high-energy synchrotron radiation (~100 keV), which combines the high penetration power of neutrons with high-momentum space resolution. The penetration depth of 100-keV x rays in YBCO is of the order of 1 mm. This assures that we probe the bulk properties of the samples and are insensitive to oxygen diffusion in and out of the surface. We present temperature scans of the structure factors of the superstructures, determine their phase boundaries, and the nature of the ordering. We show that the superstructures including ortho-V and ortho-VIII, which Beyers *et al.*[20] have observed by electron microscopy, represent bulk structural phases. From the stability of a superstructure ranging eight unit cells, the relevancy of long-range Coulomb interactions is demonstrated and we conclude, together with computer simulations,[34] that these long range Coulomb interactions lead to frustration preventing the formation of long range order.

The layout of the paper is as follows. In Sec. II, we supply information about the sample preparation Sec. (II A) and the experimental setup (II B). The experimental results are presented in Sec. III.

In Secs. III A–III D, we present the ordering properties of the ortho-II, -III, -V, and -VIII superstructures, including their temperature behavior. In Sec. IV, we discuss our experimental structural results in relation to other structural findings and their importance for charge transfer, and to theoretical model descriptions. A concluding summary is given in Sec. V.

II. EXPERIMENTAL DETAILS

A. Sample preparation

The single crystals used to study the different superstructure phases and establish the phase diagram were grown in yttria-stabilized zirconia crucibles by a flux growth method[35] using chemicals of 99.999% purity for Y_2O_3 and CuO, and 99.997% for $BaCO_3$. The impurity level of the crystals has been analyzed by inductively coupled plasma mass spectroscopy. The Zr content of the crystals was found to be less than 10 ppm by weight. The major impurities were Al, Fe, and Zn, the sum of which amounts to less than 0.2% atom per unit cell. When optimally doped ($x=0.93$) these crystals have $T_c=93.2$ K and the width of the 10–90% diamagnetic response is $\Delta T_c=0.3$ K. All the crystals are platelike with thicknesses of 0.5–1 mm, flat dimensions of 1.5–3 mm, and weights ranging from 10 to 70 mg. The oxygen composition of the crystals was changed by use of a gas-volumetric equipment.[36,37] The technique allows to determine the oxygen composition with an accuracy better than $\Delta x=0.02$. It has been compared with the known values of the oxygen equilibrium pressure determined by Schleger *et al.*,[37], and full agreement has been established in all cases. Crystals prepared previously by the method have been examined by neutron-diffraction technique and the oxygen compositions *x* determined from crystallographic analysis of 375 unique reflections were found to be in full agreement with the values obtained from the gas volumetry.[38] For studies of the structural phase diagram a characteristic procedure to establish the superstructure is annealing at 80 °C for 10 h and cooling by 1 °C/h to room temperature where the crystal is stored for more than one week before the measurements.

B. Instrument

The experiments were performed on a triple axis diffractometer at the high-energy beam line BW5 at HASYLAB in Hamburg.[39] The setup has been described in earlier publications.[9,40] The monochromator and analyzer crystals in this experiment were either (2,0,0) $SrTiO_3$ crystals or (1,1,1) $Si/TaSi_2$ crystals.[41] Both types of crystals had a mosaic spread of ~50″ (arc sec), resulting in a longitudinal resolution of 0.0075 $Å^{-1}$ at the (2,0,0) reflection of $YBa_2Cu_3O_{6+x}$. The transverse resolution is limited by the sample mosaicity, which was in the range of 0.05°–0.1° for our samples, corresponding to ~0.0015 $Å^{-1}$ at the (2,0,0) reflection. The vertical resolution depends on the setting of the slits before and behind the sample. They were usually set to integrate the scattering over a quarter of a reciprocal lattice unit, which is 0.40 $Å^{-1}$ along the *a* and *b* axes and 0.13 $Å^{-1}$ along the *c* axis. The sample was wrapped in Al foil and mounted in a small furnace. The furnace temperature was stable within 1 °C. An inert atmosphere of 0.3 bar Ar was introduced into the furnace to prevent oxidation of the crystals. From the gas-volumetric preparations, it is established that the reduction is negligible for temperatures below 300 °C, and we observed no changes in the structural properties which could be related to a change of oxygen composition during temperature cycling at temperatures below 250 °C.

C. Analysis of superstructure data

The ortho-II superstructure reflections are well described by the scattering function

$$S(\mathbf{q})=A/[1+(q_h/\Gamma_h)^2+(q_k/\Gamma_k)^2+(q_l/\Gamma_l)^2]^y, \quad (1)$$

where q_i, $i=h$, k, l, is the reduced momentum transfer and Γ_i is the reduced inverse correlation length, related to the

correlation length ξ_i by $\xi_h = a/(2\pi\Gamma_h)$ for the a direction and analogous along b and c. Equation (1) is a 3D anisotropic Lorentzian raised to the power y. The measured intensity $I(\mathbf{q})$ is then given by

$$I(\mathbf{q}) = \int S(\mathbf{q}' - \mathbf{q}) R(\mathbf{q}') d\mathbf{q}' + B, \qquad (2)$$

the convolution of the scattering function with the resolution function $R(\mathbf{q})$. The resolution function has been approximated by a δ function in the scattering plane and a box function with a width given by the gap of the detector slits in the direction perpendicular to the scattering plane. B is a background independent of $\mathbf{q}$. The exponent y in Eq. (1) indicates the distribution of domain size, i.e., $y=1$ points to an exponential decrease of the pair correlations, for example, in the ramified clusters typically for critical fluctuations above the transition temperature. The exponent $y=2$ may result from a domain size distribution around an average value Γ_i (Ref. 42), and the asymptotic behavior for large q is in agreement with Porod's law for scattering from 3D finite-size domains with sharp boundaries. Furthermore, Bray has shown that the tail of the scattering function from a topological defect of dimension m, in a system of dimension d, is given by $S(q) \propto 1/q^{2d-m}$.[43] The relation between Γ and the peak width Δ is $\Gamma = \Delta/\sqrt{2^{1/y}-1}$. When full integration of the superstructure peak is performed perpendicular to the scattering plane by relaxing the vertical aperture, the in-plane scattering function derived from Eq. (1) is described by a Lorentzian to the power $y' = y - \frac{1}{2}$.

The ortho-III, ortho-V, and ortho-VIII superstructures are essentially 2D ordered giving rise to significant overlap of the peaks along l.[29,44,45] In this case, full integration in the vertical direction cannot be obtained when the c axis is perpendicular to the scattering plane. For the 2D ordered superstructures with finite domain size and sharp boundaries, it is expected that the scattering function in the a-b plane should be a Lorentzian to the power $y' = y = 3/2$ because the integration along c is rather incomplete, whereas it should be a simple Lorentzian ($y' = y - 1/2 = 1$) when the c direction is in the scattering plane and full integration along the a or b direction is performed.

No corrections were applied to the raw data, since both the absorption and the polarization factors have negligible influence on the scattering profiles at photon energies of 100 keV used for these experiments.[39] Neither corrections for thermal diffuse scattering nor Debye-Waller factor have been applied since their contribution to the measured intensities in the limited temperature range between room temperature and 250 °C which we studied is estimated to be small.[46]

III. RESULTS

A. The ortho-II superstructure

In samples with the compositions of $x=0.35$, 0.37, 0.42, 0.5, and 0.6, a pure ortho-II phase ordering was found, and for $x=0.62$ the ortho-II is in a mixed phase with ortho-V, as described in Sec. III C. In the ortho-II phase, superlattice reflections are located at positions of $(h+1/2,k,l)$ with h, k, and l as integers. The occurrence of superlattice reflections at every integer value of l indicates that oxygen chains of subsequent layers stack on top of each other. The pure ortho-II phase is a 3D ordered structure with anisotropic correlation length along the three crystallographic directions, which were found to depend on the oxygen composition and, as we shall show in a subsequent paper,[47] on the crystal quality and thermal treatment. The longest correlation lengths observed so far are in a twin-free crystal at the ideal composition for ortho-II phase ordering of $x=0.5$, with $\xi_a = 148$ Å, $\xi_b = 430$ Å, $\xi_c = 58$ Å.[48]

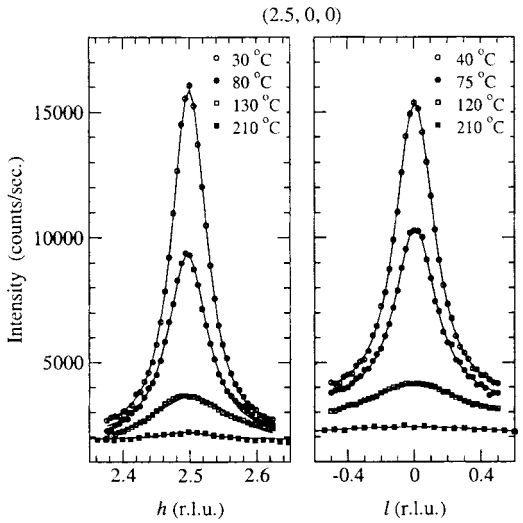

FIG. 1. Reflection profile of the (2.5,0,0) reflection measured along h and l at selected temperatures. The lines are fits to a Lorentzian function raised to the power y' [see Eq. (1) and Fig. 2].

In order to reveal the influence of the stoichiometry on the ordering properties, the ortho-II phase was investigated at a stoichiometry away from the ideal composition of $x=0.5$. Here we report in detail on the temperature dependence of the $x=0.42$ sample. Scans along h and l of the $x=0.42$ sample at selected temperatures are shown in Fig. 1. The data were fitted to a Lorentzian function raised to a power y' as described in Sec. II C. The fit parameters are plotted versus temperature in Fig. 2. The widths of the ortho-II superlattice reflections at room temperature are tabulated in Table I and are about a factor 2 broader than the width found in our twinned $x=0.50$ sample (cf. Fig. 10 below). The line shape of the superlattice peaks of the $x=0.42$ sample at room temperature is not described by a Lorentzian squared, as was found for the $x=0.5$ sample,[9] but a Lorentzian raised to a power of $y=1.85$. Both the larger width of the superlattice reflection and the lower exponent of the Lorentzian indicate more disorder in the ortho-II phase compared to the $x=0.5$ composition.

On heating the peak intensity is constant below 40 °C and starts to decrease above this temperature. At 75 °C it shows an inflection point, as determined by the minimum of the normalized slope (dI/dT) of the peak intensity, plotted in the inset, which indicates the crossover from static order to critical fluctuations. These fluctuations extend to rather high temperatures. Even at 240 K, the highest temperature accessible with our furnace, an appreciable amount of intensity due to

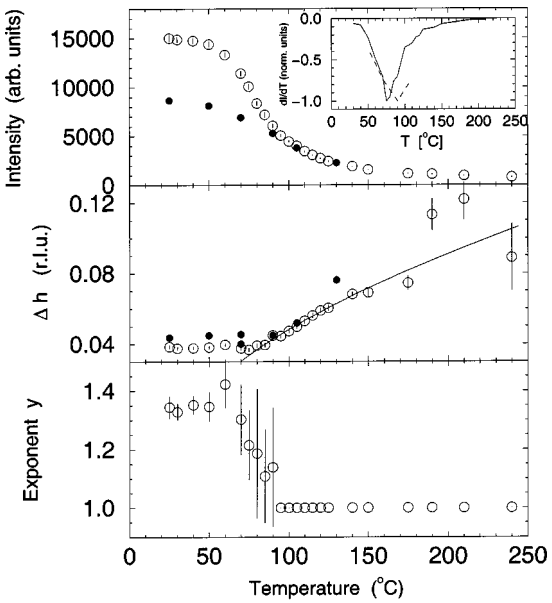

FIG. 2. Top: Peak intensity of the (2.5,0,0) reflection of the $x=0.42$ sample. Open symbols mark the data obtained during heating, filled symbols those from cooling. The inset shows the slope of the data for heating (solid line) and those for cooling (dashed line) normalized to unity. Middle: Half width at half maximum (Δh) of the superstructure reflection. The line is a fit to the critical behavior of a three-dimensional Ising model. Bottom: Exponent of the Lorentzian scattering function. The exponent of the data above 90 °C is fixed to $y'=1$.

ortho-II fluctuations is still measurable. The peak width, determined by h scans on the (2.5,0,0) reflection, starts to broaden at 80(5) °C. This temperature agrees rather well with the change in curvature of the intensity, i.e., the minimum in the slope dI/dT. Above 80(5) °C, the temperature dependence of the line width (Δh) is well described by the critical exponent $\nu=0.63$ for the 3D Ising model:

$$\Delta h(T)=\Delta h_0|T-T_c|^{\nu}. \tag{3}$$

This behavior is shown in the middle part of Fig. 2. The bottom part of Fig. 2 shows the temperature dependence of the line-shape exponent of the ortho-II reflection. Between room temperature and 60 °C the line shape remains unchanged and is described by a Lorentzian with the exponent $y'=1.35$; between 70 °C and 90 °C, the exponent decreases to 1 and was fixed to this value above 90 °C. This crossover in the line shape from a Lorentzian raised to a power of $y'=1.35$ in the low-temperature phase to a simple Lorentzian at higher temperature indicates the transition from a nearly ordered phase with antiphase domain walls separating ordered regions (cf. Sec. II C) into the regime of critical fluctuations.

On cooling we observe that the data are well reproduced down to temperatures of 80 °C. Below that temperature the peak intensities remain smaller than on heating and the peak width remain broadened, indicating critical slowing down. However, the integrated intensity is found to be the same during heating and cooling. Since the results of the ortho-II superstructure ordering indicate that internal superstructure order is established inside the finite size domains,[10] it is appropriate to define a transition temperature T_{OII}. It is natural to define the onset of critical fluctuations as the transition temperature, which can be determined, as shown above, by the minimum in the differentiation of the peak intensity, by the onset of peak broadening, and by the crossover of the exponent y' to 1. All three quantities are in agreement to within ±5 °C, so that we find for the $x=0.42$ sample $T_{OII}=80(5)$ °C. It is interesting to note that for all samples we have studied the peak intensity and the peak width below 40 °C are constant within the time period studied, which is explained by the slow kinetics of oxygen below this temperature. The ordering pattern at these temperatures is frozen in, since the activation energy of about 1.4 eV is too high for oxygen to be mobile.[9]

The investigation of the temperature dependence of the ortho-II phase at $x=0.42$ exhibits a similar behavior as found for a sample with $x=0.50$. The only difference is a shift in the transition temperature and a higher degree of disorder at room temperature for the $x=0.42$ sample, resulting in more diffuse superlattice reflections. However, since the main features of the transition, discussed above, remain the same we conclude that a commensurate oxygen stoichiometry has only a minor effect on the ordering properties of the superlattice and that a different mechanism than a noncommensurate stoichiometry prevents the formation of long-range order.

We furthermore surveyed the q space for correlations of different types of ordering, in particular at the low doped sample of $x=0.35$, but were unsuccessful to find correlations of the herringbone-type, $\sqrt{2}a\times 2\sqrt{2}a\times c$ or $2\sqrt{2}a\times 2\sqrt{2}a\times c$, structures which were observed in other studies by electron,[18,31,49] x-ray,[50] and neutron diffraction.[32]

TABLE I. Tabulated values of the transition temperatures in reciprocal lattice units on heating and the inverse correlation length in °C at room temperature along h, k, and l of the oxygen-ordering superstructures.

x		Δh	Δk	Δl
Ortho-II	T_{OII}			
0.35	85(10)	0.057(7)		0.38(6)
0.37	95(10)	0.048(6)	0.010(8)	0.19(2)
0.42	75(5)	0.031(1)	0.0097(4)	0.14(2)
0.5	125(5)	0.0104(5)	0.0042(4)	0.069(7)
0.6		0.0105(3)	0.0058(1)	0.064(1)
0.62	100(15)	0.03(2)	0.007(1)	
Ortho-III	T_{OIII}			
0.72	50(5)	0.0310(5)	0.0124(6)	
0.77	75(5)	0.031(1)	0.0091(1)	
0.82	60(20)	0.056(6)	0.021(3)	
Ortho-V	T_{OV}			
0.62	75(5)	0.058(8)	0.009(1)	
Ortho-VIII	T_{OVIII}			
0.67	42(5)	0.053(2)	0.012(2)	

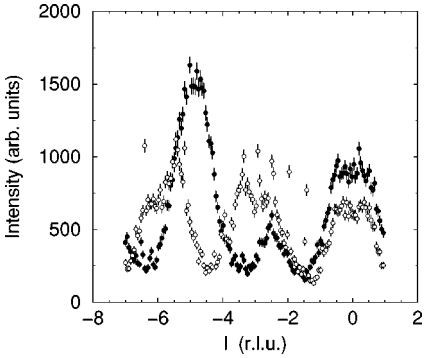

FIG. 3. Ortho-III superlattice reflections at the oxygen composition $x=0.72$ at room temperature, scanned along (7/3,0,l) (open circles) and (8/3,0,l) (filled circles).

B. The ortho-III structure

The ortho-III phase is found at the oxygen compositions of $x=0.72$, 0.77, and 0.82. A crystal prepared with $x=0.87$ showed no sign of any superstructure oxygen ordering. At these oxygen compositions the ortho-III phase is formed by the sequence (110) of two full (1) chains and one empty (0) chain. Accordingly, the size of the unit cell is tripled along the *a* direction and the diffraction pattern shows two superstructure reflections along *h* between the fundamental Bragg peaks, as shown in earlier publications.[29,44,45,51] The ortho-III superlattice peaks are well defined in the *a*-*b* plane, but like all superstructures due to oxygen ordering in YBCO, broadened due to finite domain sizes. The widths for the three compositions can be found in Table I. The smallest values, which have been reported previously by Schleger *et al.*,[45] are found in the $x=0.77$ crystal with $\Delta h=0.031(1)$ and $\Delta k=0.0090(2)$. The diffraction peaks measured along *h* and *k* exhibit a simple Lorentzian line shape. In contrast to the ordering in the *a*-*b* plane, the *l* dependence of the diffracted intensity shows only a broad modulation, with maxima occurring at noninteger values of *l* and peak width corresponding to more than one reciprocal lattice unit, as shown in Fig. 3. The large width of these reflections along *l* shows that the oxygen ordering of subsequent planes is only weakly correlated and the ordering takes place only in the *a*-*b* plane. Thus, in contrast to the ortho-II phase, which is 3D ordered, the ortho-III phase is essentially a 2D ordered superstructure. While it is obvious that an appreciable amount of disorder leads to these broad reflection profiles along *l*, the detailed line shape is still debated. Plakhty *et al.* model the *l* dependence at room temperature very well with a periodic function that, in principle, shows maxima at every integer number of *l*.[29,44] A different origin for the *l* modulation has been recently suggested by Islam *et al.*[14] who found a very similar modulation at $x=0.63$ for the ortho-V phase (described in detail in Sec. III C). By Fourier transformation of the intensity modulation measured along *l* at 14 K, they show that not only the basal planes contribute to this modulation but also the copper-oxygen planes. In fact, the distance of the origin to the first maximum corresponds to the correlations between the basal plane and the CuO plane, the one to the second maximum to correlations between the basal plane and the BaO plane. Thus, correlations between three different planes might give rise to the *l* modulation. However, a quantitative analysis for *l* scans with different values of *h* and *k* remains to be performed.

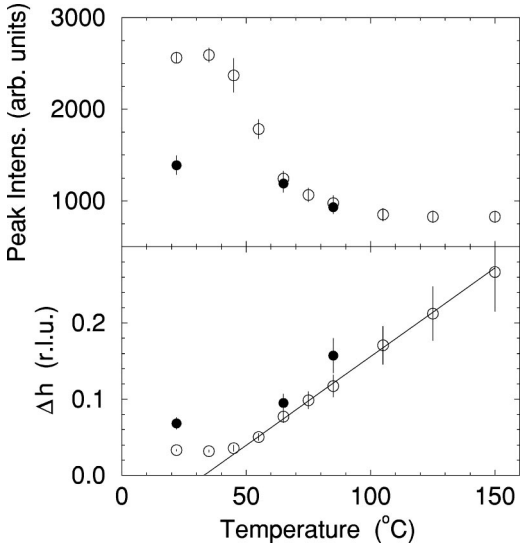

FIG. 4. Ortho-III transition at the oxygen composition $x=0.72$, where the peak intensity (top) and the peak width (bottom) of the (8/3,0,5) reflection were measured by *h* scans. The open circles show the heating data and the filled circles the data during cooling. The line in the lower graph shows the behavior described by the 2D Ising model above the transition temperature.

For the crystal with composition $x=0.72$, a detailed study of the temperature dependence of the ortho-III phase including the peak intensity as well as the correlation length is shown in Fig. 4. For this crystal the (8/3,0,5) reflection was scanned along *h* at various temperatures. Similar to the transition of the ortho-II phase, the peak intensity and peak width are frozen at temperatures smaller than 35 °C. Above this temperature, the peak intensity decreases rapidly and the broadening of the peak width along *h*, shown in the bottom part of Fig. 4, indicates the onset of critical fluctuations. Fitting the temperature dependence of the peak width to Eq. (2) a critical exponent of $\nu=0.92(8)$ is obtained, with a transition temperature of $T_{OIII}=48(5)$ °C. This value for the critical exponent is in good agreement with the theoretical value of $\nu=1$ for the 2D Ising model and consistent with a 2D character of the ortho-III order.

C. Ortho-V

The investigation of a crystal prepared with the oxygen composition of $x=0.62$ shows a mixture of ortho-II and ortho-V phases at room temperature. This is revealed by the observation of diffuse peaks at positions of $h=2.4$, 2.5, and 2.6 as shown in Fig. 5. The peak at $h=2.5$ results from the ortho-II structure, and the peaks at $h=2.4$ and $h=2.6$ are consistent with a unit cell which is enlarged five times in the *a* direction, i.e., the ortho-V structure. The two small peaks seen in the *h* scan in Fig. 5 at $h=2.23$ and $h=2.83$ are an Al-powder line and possibly a grain of an unknown phase oriented with the lattice, respectively. The hump at $h=2.83$

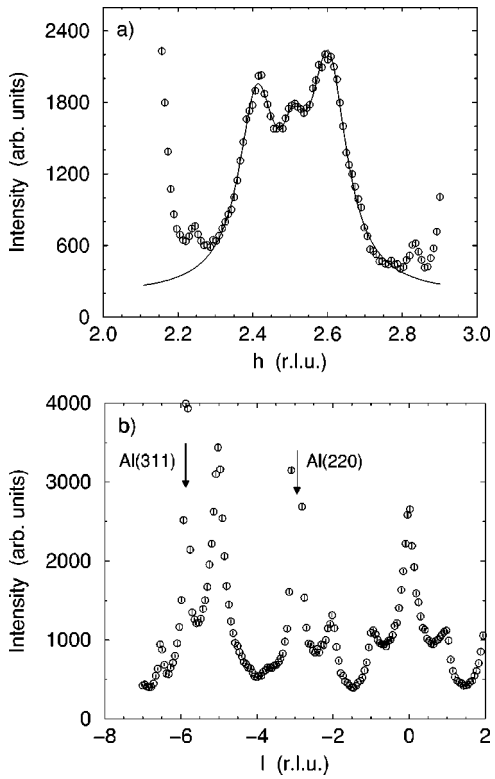

FIG. 5. Scans along h (a) and l (b) at room temperature for a crystal prepared to $x=0.62$. The peaks in the (h,0,0) scan at $h=2.4$ and $h=2.6$ result from the ortho-V phase. The scattering signal at $h=2.5$ indicates the presence of the ortho-II phase. The weak peak at $h=2.23$ is an Al-powder line originating from the sample holder and the bump at $h=2.83$ is unidentified. At $h=2.1$ and $h=2.9$, tails of the fundamental Bragg reflections are observed. The lower panel shows a (2.5,0,l) scan. The arrows indicate the position of Al-powder lines.

has also been observed when the same crystal was prepared with other oxygen compositions (compare with Fig. 7 and Ref. 45). A similar diffraction pattern, consistent with a mixture of ortho-II and ortho-V, has been observed in all (h 0 l) scans performed with $1 \leqslant h \leqslant 4$ and $l=0$, 3, 5, 6, 7 (eight scans in total). However, none of these scans showed a peak at position $\mathbf{Q}=(\frac{1}{5},0,l)$. This is explained by the structure factor calculations of the superlattice peaks from the ideal ortho-V ordering sequence (10110) shown in Ref. 13. The intensities of the peaks at (1/5, 0, 0) are indeed much smaller than the ones at (2/5,0,0) and (3/5,0,0). However, this model takes into account only the oxygen order and, as discussed in Sec. I, the superlattice peaks are caused by both the oxygen order and the cation displacements. These displacements and the pronounced disorder may change the intensities and reduce them further. Interestingly, an inelastic neutron-scattering study of an $x=0.60$ sample revealed a signal around the (4,0,0) reflection with an ordering wave vector of $\mathbf{Q}=(0.2,0,0)$ at 10 K, which is associated with a dynamic charge-density wave in the material.[15] In principle, such a charge-density wave should be observable with x rays as well[16] and would result in peaks at $h=2.2$ and 2.8 in our spectrum shown in Fig. 5. However, since the charge-density wave detected with neutrons was found to be a purely dynamic mode of oxygens, the intensity will be very weak compared to the elastic scattering due to the static oxygen ordering. In particular at room temperature, the lowest temperature accessible in our experiment, the intensity due to the charge-density wave is reported to be rather diffuse,[15] and therefore even more difficult to observe.

Due to the heavy overlap of the peaks from the two phases, it is difficult to determine the peak shape and width. However, analysis of the ortho-II and ortho-V peaks using Lorentzian profiles gave the following width at room temperature: $\Delta h=0.040(28)$, $\Delta k=0.0078(16)$, $\Delta l=0.12(3)$ for ortho-II; and $\Delta h=0.058(10)$, $\Delta k=0.0096(19)$ for ortho-V (see also Table I). The scan along l at (2.5,0,l), shown in Fig. 5, exhibits the intensity modulation well known for 3D ordering in the pure ortho-II phase, with maxima at every integer value of l. The overlap of the peaks originating from the ortho-V phase with the reflections from the ortho-II phase does not allow to determine the correlations of the ortho-V phase along the c -axis independently. However, an x-ray study of charge localization at the oxygen content of $x=0.63$ reveals a pure ortho-V phase, not mixed with an ortho-II phase.[14] Here a scan along (4.4,0,l) reveals a very similar diffraction pattern as we find for the ortho-III phase shown in Fig. 3. As discussed in the preceding section such a pattern was indicative of very weak correlations along the l direction of a 2D ordered structure.

The competition between ortho-II and ortho-V ordering is demonstrated most clearly by the temperature dependence of the mixed phase, which was measured by h scans between the (2,0,0) and the (3,0,0) Bragg reflections and the diffraction pattern was fitted to three Lorentzians with fixed positions at 2.4, 2.5, and 2.6. Interestingly, the balance between the phase mixture is affected significantly by raising the temperature as shown in Fig. 6. While the ortho-V correlations disappear between 50 °C and 70 °C, the ortho-II reflection gains intensity, which indicates that the ortho-II correlations are more stable with increasing temperature than the ortho-V correlations. During the cooling cycle the ortho-II correlations dominate the diffraction pattern, while the scattering due to ortho-V correlation is not recovering with decreasing temperature. This behavior is easily explained by the slow ordering kinetics at low temperatures.[9,10] During the cooling process the ortho-II correlations start to form, while the ortho-V correlations are still unstable. Only at a lower temperature the ortho-V phase is more stable than the ortho-II phase. However, at this low temperature the ordering kinetics is so slow that ortho-V domains are unable to grow within the 1 h time period of the experiment.

D. Ortho-VIII

Figure 7 shows h and l scans for the oxygen composition $x=0.67$. The h scans along (h,0,0) with $2<h<3$ reveal diffuse superlattice peaks at $h=2.382(4)$ and $h=2.627(3)$. The peak positions and profiles have been fitted to two Lorentzians giving a width of $\Delta h=0.053$. The peaks are also localized in the transverse direction with a width of $\Delta k=0.013(2)$. The modulation of the intensity for a scan along l [Fig. 7(b)] has a similar q dependence as the corresponding

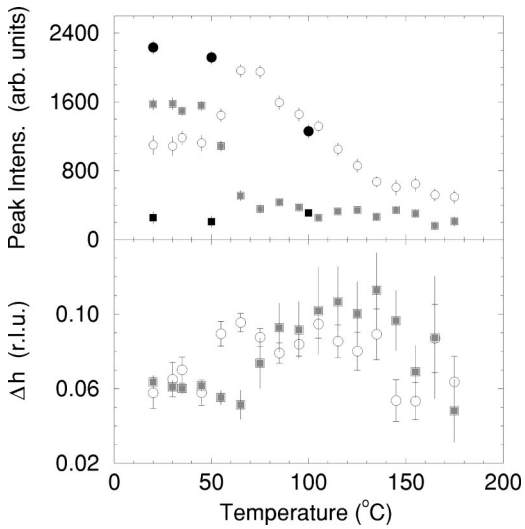

FIG. 6. Temperature dependence of the mixed phase of ortho-II and ortho-V at the oxygen composition of $x=0.62$. The top part shows the peak intensity of the ortho-II reflections (circles) and the ortho-V reflections (squares). Open and gray shaded symbols mark the data obtained during heating, the black filled symbols the cooling data. The bottom part of the figure shows the half width at half maximum (Δh) of the reflections of the two phases along h.

scan for the ortho-III phase, shown in Fig. 3. Thus, there are no well-defined peaks along l, indicating essentially 2D ordering with substantial disorder in the stacking of full and empty chains along the c direction. Similar superlattice peaks

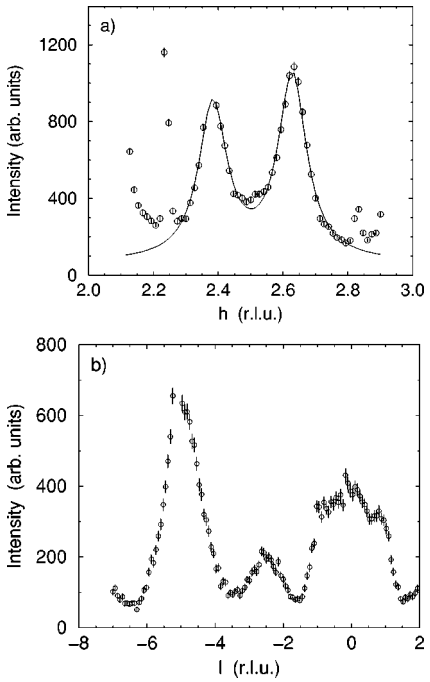

FIG. 7. Scan along (h,0,0) (a) and (2.63,0,l) (b) in a crystal with oxygen concentration of $x=0.67$ at room temperature. The h-scan shows peaks at approximately $h=2\frac{3}{8}$ and $h=2\frac{5}{8}$, indicating the ortho-VIII phase. The peak at 2.23 is an Al-powder line. The line shown together with the h scan is a Lorentzian fit. The variation of the diffracted intensity along l is only weakly q dependent and similar to that of the ortho-III phase.

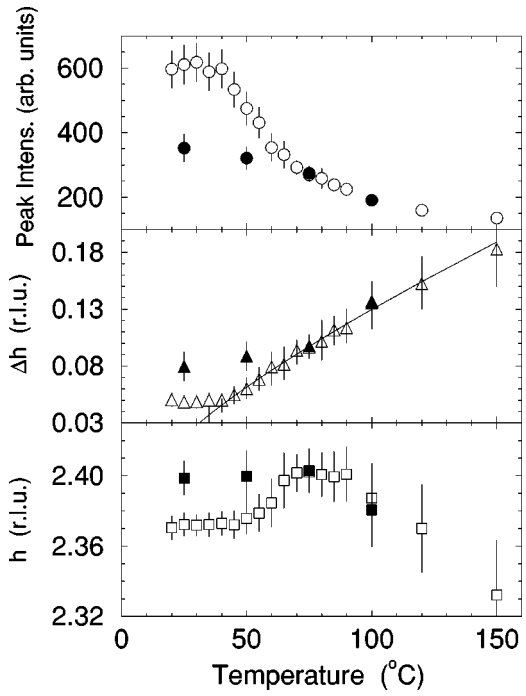

FIG. 8. Temperature dependence of the ortho-VIII phase at $x=0.67$ measured by h scans close to $(2\frac{3}{8},0,3)$. The top figure shows the peak intensity, the middle part the half width at half maximum together with a fit to a critical behavior according to Eq. (3) with $\nu=0.79(3)$, and the bottom the peak position. The shift in the peak position indicates a transformation from ortho-VIII to ortho-V structure between 50 °C and 70 °C. At 150 °C the peak position corresponds to the ortho-III structure.

have been observed at positions in reciprocal space of (h,0,3) and (h,0,5) with $2\leqslant h\leqslant 3$. The superstructure peak positions at modulation vectors with $nh_m=0.382$ and 0.627 are close to the expected values $nh_m=3/8$ and 5/8 for a superlattice with a unit cell of $8a\times b\times c$, i.e., the ortho-VIII phase. The expected sequence of full and empty chains of the ideal ortho-VIII structure is (11010110). Calculating the intensities of the superlattice peaks for this ideal case one finds that the observed peaks at $nh_m=3/8$, and 5/8 are the strongest, the peaks at $nh_m=2/8$, 4/8 and 6/8 are about one order of magnitude smaller, and the ones at $nh_m=1/8$ and 7/8 are about two orders of magnitude smaller (compare with the presentation in Ref. 13). Due to the weak ordering it is unlikely that the smaller superlattice reflections can be observed.

The temperature dependence was measured by h scans at the $(2\frac{3}{8},0,3)$ peak position and the results are shown in Fig. 8. The onset of broadening of the superstructure peaks takes place at $T_{OVIII}=42(5)$ °C. The temperature dependence of the peak width above the transition temperature is described by the critical exponent of $\nu=0.79(3)$ as shown in the middle part of Fig. 8. This value is between the exponent of 0.63 for the 2D and 1 for the 3D Ising model. Another interesting feature of this phase transition is revealed by the inspection of the peak position. When the temperature exceeds 50 °C the peak position changes continuously from $h=2.372$ to $h=2.4$, which corresponds to the position of the ortho-V phase. Above 90 °C the peak shifts gradually to $h=2.33$ at 150 °C, the location of the peaks of the ortho-III structure.

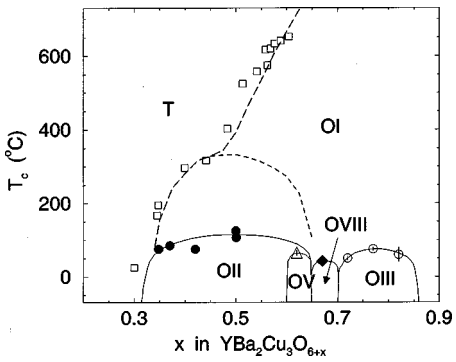

FIG. 9. The structural phase diagram of YBCO. The structural phases and their transition temperatures are labeled: tetragonal (T), ortho-I (OI, □), ortho-II (OII, ●), ortho-III (OIII, ○), ortho-V (OV, △), and ortho-VIII (OVIII, ◆). Solid lines are guides to the eye. The dashed lines are predictions from the ASYNNNI model. The data for the T-OI transition (box) are from Andersen *et al.* (Ref. 36). The T_{OII} transition temperatures for $x=0.35$ and $x=0.36$ are from Poulsen *et al.* (Ref. 40), the upper data set for $x=0.50$ is from Schleger *et al.* (Ref. 9), and the T_{OIII} transition temperature at $x=0.77$ is from Schleger *et al.* (Ref. 45).

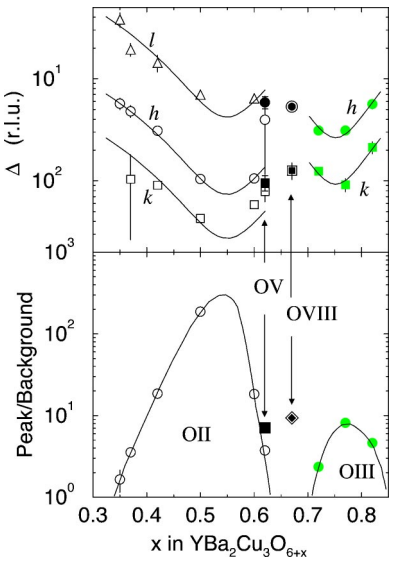

FIG. 10. Top: Half width at half maximum (Δ) at room temperature for the indicated structures as function of oxygen content. Bottom: peak to background ratio. All lines are guides to the eye.

Upon cooling the data are reproduced down to 75 °C, at lower temperatures the peak intensity is significantly reduced compared to the heating data and the structure freezes into the ortho-V phase.

E. The oxygen-ordering phase diagram

From the transition temperatures obtained in the present and previous studies[9,40,45] using hard x-ray diffraction and the same type of crystals, we may establish phase lines for the oxygen superstructure ordering. Combining these data with the transition temperatures T_{OI} of the phase transition from the tetragonal to the orthorhombic ortho-I phase, obtained by neutron powder diffraction,[36] we may construct the structural phase diagram of oxygen ordering in YBCO, shown in Fig. 9 and Table I. In the figure are also included the phase transition temperatures T_{OI} and T_{OII}, predicted by Monte Carlo simulations[52] based on the asymmetric next-nearest-neighbor interaction (ASYNNNI) model[53] with *ab initio* interaction parameters.[54]

The only true equilibrium structures are the ortho-I phase and the tetragonal phase, all superstructures formed by oxygen ordering do not show long-range ordering. Within the temperature range studied, the tetragonal phase is the only one observed for $x<0.35$. Below the tetragonal to orthorhombic phase transition temperature the 3D ordered ortho-I phase always develops, and it is the only structure observed for $x>0.82$. For $0.35\leqslant x<0.62$, the 3D short-range-ordered ortho-II phase is the only stable superstructure. Similarly, a single phase ortho-III structure with 2D finite-size ordering is observed for $0.72\leqslant x\leqslant 0.82$. At intermediate compositions a mixed phase of ortho-II and ortho-V is found at $x=0.62$, and ortho-VIII is found at $x=0.67$ in crystals that have been slowly cooled to room temperature as described in Sec. II A. Both the ortho-V and the ortho-VIII structures are essentially 2D ordered and have finite size ordering. During heating the ortho-V structure transforms into ortho-II and it does not recover on cooling within 1 h. Above room temperature the ortho-VIII structure transforms gradually first into ortho-V and then into ortho-III. On subsequent cooling the ortho-V superstructure is recovered and remains stable within the 1 h time period of the measurements.

The line shape of the superstructure reflections is in most cases well described by a simple Lorentzian ($y=1$). Only for the ortho-II phase between $0.42\leqslant x<0.62$ a Lorentzian raised to a power larger than 1 is found. At the low oxygen side of the ortho-II phase $x\leqslant 0.35$, the small peak to background ratio (see bottom part of Fig. 10) does not permit the determination of the exponent of the Lorentzian. The domain size of the superstructures depends strongly on the crystal quality[47] and the annealing times. However, for the present high-quality crystals, which have been annealed by the standard procedure for studies of the phase diagram (described in Sec. II A), we expect that the domains are at the late state of growth and therefore only weakly time dependent.[9,10] On this basis, we consider the results presented in Sec. III of the peak widths measured at room temperature after the initial thermal preparation as saturation values. The widths of the superlattice peaks measured at room temperature along the three axis of reciprocal space as function of oxygen composition are shown in Table I and depicted in Fig. 10 (top). The parallel lines (guides to the eye) in the logarithmic plot observed in the ortho-II phase as well as in the ortho-III phase show that the ratio of the anisotropy is constant within a given structural phase. For the ortho-II phase, we find the following ratios of the inverse correlation lengths at room temperature: $\Gamma_h/\Gamma_k=2.7(6)$ and $\Gamma_l/\Gamma_k=15(2)$. The a-b plane ratio seems to be independent also of the type of structure, since the ratio for the ortho-III phase, $\Gamma_h/\Gamma_k=2.9(4)$, is in good agreement with the value of the ortho-II phase. This implies that the domain pattern in the a-b plane scales in both the ortho-II and the ortho-III phases, and in ortho-II the scaling is extended to 3D. The peak intensities cannot be

compared directly because different crystals and instrumental settings have been used. However, the peak intensity normalized to the background, shown in the bottom part of Fig. 10, is essentially an independent parameter for the ordering properties. From this normalized peak intensity and the data of the peak width, it is clear that the optimal superstructure order parameter is found close to $x=0.55$.

The oxygen composition x of all the ordered phases deviates systematically from the ideal composition of these phases. For example, the longest correlation lengths for the ortho-II phase are likely to be at $x\simeq 0.55$. Unfortunately no data points are available at this composition. Theoretically one would expect the best ortho-II order for $x=0.50$. This deviation is even more significant for the ortho-III phase, which is expected at $x=0.67$, but observed around $x\simeq 0.77$. Thus, the deviation from the ideal composition increases with increasing chain density and the amount of oxygen atoms occupying sites on the empty chains at room temperature can be estimated to be about 10% for ortho-II and 30% for ortho-III.

IV. DISCUSSION

A. Experimental results

It has been known for several years that the ortho-II and ortho-III superstructures are bulk structural phases of finite-size domains. Several other superstructures have been suggested, mainly from electron microscopy. In the present paper, we have shown that also the ortho-V and ortho-VIII correlations observed by electron microscopy result from bulk structural ordering, but we found no evidence for the ortho-IV phase. However, we recognize in particular the early electron microscopy results obtained by Beyers *et al.*[20] which are in close agreement with our room-temperature data. Beyers *et al.* observe the ortho-II and ortho-III superstructures in the same composition range as in our studies. Furthermore, they found coexistence of ortho-II and ortho-V at $x=0.65$, and a structure similar to the ortho-VIII phase, which they call a ''(0.37 0 0)'' structure, at $x=0.71$.

Beyers *et al.* attributed the clear disagreement between the observed oxygen compositions and the stoichiometries of the ideal superstructure phases to gradients in the oxygen content of the sample, which might be different on the surface and in the bulk material. In our experiment such differences can be ruled out. We conclude that this deviation is an intrinsic property of the oxygen-ordering mechanism. It is possible that the phase lines between the superstructure phases are in fact tilted, and only at zero temperature the ideal oxygen stoichiometry of the superstructure phases is found. However, this will never happen because the oxygen ordering kinetics is very slow at the temperatures where the superstructures become stable, and the movement of Cu-O chains freeze effectively below approximately 40 °C.

Beyers *et al.* interpret the mixing of ortho-II and ortho-V phases at $x=0.65$ as a phase separation, which leads to the 60-K plateau.[20] Our investigation of the temperature dependence together with the studies of the ordering kinetics[9,10] may lead to a different conclusion. During the cooling of a sample with an oxygen content of $x=0.62$ (in the case of Beyers *et al.* $x=0.65$), oxygen starts to order in the ortho-II phase. The relatively high temperature enables a fast growth of ortho-II domains. At lower temperature the ortho-V phase becomes stable, but now at temperatures just above room temperatures the growth of ortho-V domains is slow. A full transformation into the ortho-V phase cannot be precluded but it is very time consuming. Therefore, we suggest that domains of the complex ortho-V superstructure start to grow inside the ortho-II structure and a mixed phase, rather than phase separation, results.

From studies of the oxygen-ordering properties, it has become clear that the finite size of the ortho-II superstructure results from formation of antiphase boundaries that limit the domain growth due to slow kinetics of moving long Cu-O chains. The reason for this has been discussed by Schleger *et al.*,[9] and it was speculated that random fields introduced by impurity defects in the crystal stabilize the antiphase domain walls and prevent formation of long-range order. This is corroborated by the present studies and additional studies of the ordering kinetics.[10] However, the observation of superstructures extending over eight unit cells shows the importance of long range interactions for the ordering mechanism. That these long-range interactions play a significant role for the finite-size ordering has recently been established by model simulations.[34] and will be discussed further below. For the ortho-III, ortho-V, and ortho-VIII superstructures, the small 2D domains indicate that the ordering resembles a random faulting sequence of ortho-II and ortho-III. Khachaturyan and Morris[55] have suggested that this is a likely ordering scheme, and they have calculated structure factors which are qualitatively similar to those observed at room temperature in our experiments. However, the fact that the ortho-V and ortho-VIII superstructures only appear when they are slowly cooled indicates that the long-range interactions tending to form these superstructures become effective at low temperatures, but the slow oxygen-ordering kinetics for movement of long Cu-O chains prevent that well-defined domains are formed. As mentioned in Sec. II C, we would expect a diffraction profile of a Lorentzian to the power $y'=y=3/2$ from 2D domains with sharp boundaries when the integration along the c axis is incomplete. The observation that all the superstructure peaks of the ortho-V, ortho-VIII, and ortho-III peaks are described by Lorentzian profiles suggests that these superstructures have a more fuzzy type of boundaries than the ortho-II domains.

Generally, there is significant hysteresis in the superstructure ordering when the temperature is cycled through the phase transitions. The ortho-II and ortho-III superstructures are reestablished during cooling from the ortho-I phase within 1 h. However, the ortho-V phase (mixed with ortho-II) and the ortho-VIII do not recover during cooling within this short time period. Instead, the less complex superstructures, ortho-II and ortho-V develop, respectively. It is obvious that the superstructure ordering does not represent equilibrium phases, and it cannot be precluded that more complex superstructures may be formed by very long-time annealing at an appropriate temperature or in crystals that are even more perfect than the present ones. According to Ostwald's step rule for phase transformations, metastable phases

may be formed, before the system finally transforms into the stable phase, as long as nucleation centers with a similar structure such as the metastable phases are present. In our case, the ortho-II and ortho-III phases might be nucleation centers for the ortho-V phase, which in turn, at $x=0.67$, is metastable and serves as a nucleation center for the ortho-VIII phase (see Fig. 8). Thus, although we have been able to define unique transition temperatures, at least for the ortho-II superstructure phase, it is questionable whether we have established a phase diagram in the usual sense. This may explain why the phase diagram does not comply with Gibb's phase rule.

The 3D ordered superstructures with unit cells $2\sqrt{2}a \times 2\sqrt{2}a \times c$ and $\sqrt{2}a \times 2\sqrt{2}a \times c$, the so-called herringbone structure, have been observed by electron microscopy, and one group has reported on these structures by neutron-[32] and x-ray diffraction[50] techniques on single crystals with composition $x=0.35$. However, no other experiments with bulk structural techniques could confirm these results. Bertinotti *et al.*[56] and Yakhou *et al.*[57] have shown that the reflections of the herringbone type can be assigned to $BaCu_3O_4$ grains in the crystals. Krekels *et al.*[58,59] attribute the $2\sqrt{2}a \times 2\sqrt{2}a \times c$ structure to distortions of the CuO_5 pyramids in the CuO_2 planes, and Werder *et al.*[60] suggest that they could result from ordering of copper and barium vacancies in the lattice. The consensus from these and several other studies is therefore that the $2\sqrt{2}a \times 2\sqrt{2}a \times c$ and the herringbone-type structures are not oxygen-ordering superstructures in YBCO. If they were, it is peculiar that they have 3D long-range order while the Cu-O chain ordering develops only finite-size domains. Also, we have found no evidence of them at any composition x in the present hard x-ray-diffraction studies on carefully prepared high-quality single crystals. However, as previously mentioned this type of ordering has been identified as genuine oxygen superstructures in $NdBa_2Cu_3IO_{6.50}$.[33]

B. Significance for superconductivity

The significance of the oxygen ordering for charge transfer and superconductivity is obvious from many studies. Chemical bond considerations combined with structural[11,12] and spectroscopic studies[61,62] have shown that the basal plane copper in undoped $YBa_2Cu_3O_{6+x}$, $(x=0)$ is monovalent and that simple oxygen monomers, i.e., Cu-O-Cu, will not give rise to charge transfer. However, charge transfer is observed for larger x where Cu-O chains are formed. Cava *et al.*[11] and Tolentino *et al.*[61] have established that an increasing amount of oxygen gives rise to a charge transfer to the CuO_2 planes, which is in good agreement with the well-known plateau variation of T_c with $T_c=58$ K around $x=0.5$ and $T_c=93$ K close to $x=1$. Relating the oxygen ordering to the variation of T_c observed, e.g., by Cava *et al.*[11] we find that the 58-K plateau is identical to the stability range of the ortho-II superstructure, the rise in T_c from the 58-K to the 93-K plateau takes place at values of x where the ortho-V/II, ortho-VIII, and ortho-III structures are found, and the 93-K plateau coincides with the oxygen compositions of the ortho-I phase. Furthermore, despite the characteristic plateau variation of $T_c(x)$ in pure YBCO, it has been shown that the hole doping p determined from neutron-diffraction data combined with bond valence analysis gives rise to the generic parabolic variation of $T_c(p)$ in oxygen as well as calcium doped $Y_{1-y}Ca_yCu_3O_{6+x}$.[12]

The significance of the ortho-II ordering for superconductivity has been shown directly by Veal *et al.*[6] and Madsen *et al.*[8] Both groups have shown that T_c is significantly reduced just after a quench and increases with time towards the equilibrium values with a thermal activated time constant. The conclusion, which may be drawn from these experiments and the present structural data, is that the formation of ortho-II superstructure is decisive for the charge transfer and T_c. When the sample is quenched from temperatures above T_{OII}, and even from the tetragonal phase, it is only the time used to quench it into the ortho-II phase that matters. A time dependent increase of T_c is observed at annealing temperatures down to 250 K. Most likely this temperature is the lower limit for local oxygen jumps which dominates the oxygen ordering at the very early time. It is unlikely that the domain wall separating antiphase domains are mobile at 250 K.

C. Relation to model calculations

From the present and previous studies, it is evident that the local oxygen-ordering properties are important for the electronic structure and the charge transfer, but the details of the local ordering phenomena are difficult to obtain directly from the diffraction experiments. Thus it is important that the data are related to a model that describes the oxygen-ordering properties adequately. The predictive power of these model studies for the structural and electronic properties is strongly depending on their ability to reproduce experimental findings, as presented in the present structural studies.

Most of the structural models are based on local effective oxygen-oxygen interactions in a 2D lattice-gas formulation.[53,63] Among the simplest models that account for many elements of the oxygen-ordering properties, such as the formation of Cu-O chains and the presence of the tetragonal, ortho-I, and ortho-II phases, is the so-called ASYNNNI model,[53] which is a 2D lattice-gas (or Ising) model with effective oxygen-oxygen pair interactions that are assumed to be independent of temperature and composition x. This model considers the Coulomb interaction between nearest- and next-nearest-neighbor oxygen atoms and accounts quantitatively[52] for the temperature and composition dependence of the experimental structural phase transition between the tetragonal and the ortho-I phases[36] (see Fig. 9) by use of interaction parameters, which are consistent with values obtained by Sterne and Wille from first-principles total-energy calculations.[54] It also predicts the existence of the ortho-II phase, but it cannot account for the additional superstructure phases, ortho-III, ortho-V, and ortho-VIII. Moreover, it predicts long-range order of the superstructure phases, which has never been obtained experimentally, and it cannot account quantitatively for the ortho-I to ortho-II phase transition temperature.

Extensions of the ASYNNNI model have been suggested to account for the shortcomings. These include an effective 3D interaction with a nearest-neighbor attractive interaction

along c,[52] effects of electronic degrees of freedom in the Cu-O chain structure,[2–4] and 2D Coulomb-type interactions of longer range than next-nearest neighbor.[13,64] The influence of including effective Coulomb-type Cu-O chain interactions extending beyond a and $2a$ has been studied analytically in the framework of a 1D Ising model.[13] Here a sequence of branching phases develops for $T \rightarrow 0$ in order to comply with the Nernst principle and stoichiometric phases at different compositions x. However, for the YBCO system it is expected that the interactions of range beyond $2a$ play a role only at low temperatures where effectively the structural ordering is frozen.

For the 2D ordering it has been argued that a single additional interaction parameter for oxygen atoms that are $2a$ apart and not bridged by copper should be sufficient.[34] This additional interaction becomes effective when Cu-O chains have already been formed, and it will act as an effective interaction between chains rather than between oxygen pairs. Studies of the ASYNNNI model extended this way do not only predict the stability of the ortho-II and ortho-III phases, which is expected by construction, but also shows that short range correlations of ortho-V and ortho-VIII are established. Furthermore, the ortho-II and ortho-III superstructures do not develop long-range order, consistent with our experimental observations. The finite-size ordering of the superstructures is therefore not necessarily a consequence of impurities or defects that pin the domain walls, but may be an intrinsic disordering property. In further agreement with the experiments, the ASYNNNI model extended with the interaction parameter acting between oxygen atoms $2a$ apart as well as the 3D model predict a significant suppression of the T_{OII} ordering temperature relative to the T_{OI} temperature which the original version failed to do (see Fig. 9). One of the major objections against the validity of the ASYNNNI model has been the assumption that the interaction parameters are independent of x. However, our data show that the ratios of the correlation lengths are indeed independent of the oxygen stoichiometry in the ortho-II and the ortho-III phases, consistent with mean-field predictions of the peak widths.[42] The ASYNNNI model is therefore a promising model for analysis of experimental results, and credible predictions about the local oxygen-ordering properties and the present experimental results can be used as a guide to further model studies.

V. CONCLUDING SUMMARY

High-energy x-ray diffraction has proven to be a unique tool for studies of oxygen-ordering properties in the orthorhombic phase of YBCO. Chain ordered superstructures of the ortho-II, ortho-III, ortho-V, and ortho-VIII types have been observed in high-quality single crystals with this bulk sensitive technique. None of the superstructures develops long-range order. Only the ortho-II phase is a 3D ordered superstructure with anisotropic correlation lengths. The ortho-II correlation lengths observed at room temperature depend on the oxygen composition (optimal for $x=0.55$), crystal perfection,[47] and thermal annealing. All other superstructures have 2D character with ordering only in the a-b-plane. The ratio of the a-b plane correlation lengths is essentially independent of the oxygen composition and the type of ordering. The transition temperatures of the superstructures are between room temperature and 150 °C. The ordering properties resulting from thermal cycling through the T_{OII} and the T_{OIII} ordering temperatures show that finite-size domains with internal thermodynamic equilibrium are formed. The domain size observed on cooling from the ortho-I phase within 1 h is significantly reduced compared to the value obtained by long-time annealing. The observation of ortho-V mixed with ortho-II and ortho-VIII superstructures shows that these superstructures are bulk properties, and that Coulomb interactions beyond next-nearest neighbors become effective close to room temperature. The ordering of the ortho-V and ortho-VIII superstructures does not reproduce when the sample is cooled from the ortho-I phase within 1 h, and it cannot be precluded that additional superstructure phases may be formed by careful annealing of high-quality single crystals. Therefore, although an unambiguous criterion has been identified for the ordering temperatures of the finite-size ortho-II and ortho-III superstructures, the resulting ''phase diagram'' is not an equilibrium phase diagram in the usual sense.

ACKNOWLEDGMENTS

This work was supported by the EC TMR—Access to Large Scale Facilities Program at HASYLAB, and the Danish Natural Science Research Council through DanSync. T.F. was supported by the Danish Technical Science Research Council. Collaboration with H. Casalta, R. Hadfield, and P. Schleger on initial studies preceding this work is gratefully acknowledged. Technical assistance from S. Nielsen, R. Novak, A. Swiderski, and T. Kracht is much appreciated.

[1] J.D. Jorgensen, M.A. Beno, D.G. Hinks, L. Soderholm, K.J. Volin, R.L. Ritterman, D.G. Grace, I.K. Schuller, C.U. Segre, K.Z. Zhang, and M.S. Kleefisch, Phys. Rev. B **36**, 3608 (1987).

[2] G. Uimin, Phys. Rev. B **50**, 9531 (1994).

[3] A.A. Aligia and J. Garcés, Phys. Rev. B **49**, 524 (1994).

[4] H. Haugerud, G. Uimin, and W. Selke, Physica C **275**, 93 (1997).

[5] H. Claus, S. Yang, A.P. Paulikas, J.W. Downey, and B.W. Veal, Physica C **171**, 205 (1990).

[6] B.W. Veal, A.P. Paulikas, H. You, H. Shi, Y. Fang, and J.W. Downey, Phys. Rev. B **42**, 6305 (1990).

[7] S. Libbrecht, E. Osquiguil, B. Wuyts, M. Maenhoudt, Z.X. Gao, and Y. Bruynseraede, Physica C **206**, 51 (1993).

[8] J. Madsen, N. H. Andersen, M. v. Zimmermann, and Th. Wolf, Risø Report R-933 (EN), 1997 (unpublished).

[9] P. Schleger, R. Hadfield, H. Casalta, N.H. Andersen, H.F. Poulsen, M. von Zimmermann, J.R. Schneider, Ruixing Liang, P. Dosanjh, and W.N. Hardy, Phys. Rev. Lett. **74**, 1446 (1995).
[10] M. Käll, M.v. Zimmermann, N.H. Andersen, J. Madsen, T. Frello, H.F. Poulsen, J.R. Schneider, and Th. Wolf, Europhys. Lett. **51**, 447 (2000).
[11] R.J. Cava, A.W. Hewat, E.A. Hewat, B. Batlogg, M. Marezio, K.M. Rabe, J.J. Krajewski, W.F. Peck, Jr., and L.W. Rupp, Jr., Physica C **165**, 419 (1990).
[12] J.L. Tallon, C. Bernhard, H. Shaked, R.L. Ritterman, and J.D. Jorgensen, Phys. Rev. B **51**, 12 911 (1995).
[13] D. de Fontaine, G. Ceder, and M. Asta, Nature (London) **343**, 544 (1990).
[14] Z. Islam, S.K. Sinha, D. Haskel, J.C. Lang, G. Srajer, D.R. Haeffner, B.W. Veal, and H. A Mook, Phys. Rev. B **66**, 092501 (2002).
[15] H. A Mook and F. Doğan, Nature (London) **401**, 145 (1999).
[16] M.v. Zimmermann, A. Vigliante, T. Niemöller, N. Ichikawa, T. Frello, J. Madsen, P. Wochner, S. Uchida, N.H. Andersen, J.M. Tranquada, D. Gibbs, and J.R. Schneider, Europhys. Lett. **41**, 629 (1998).
[17] H.W. Zandbergen, G. van Tendeloo, T. Okabe, and S. Amelinckx, Phys. Status Solidi A **103**, 45 (1987).
[18] J. Reyes-Gasga, T. Krekels, G. van Tendeloo, J. van Landuyt, S. Amelinckx, W.H.M. Bruggink, and H. Verweij, Physica C **159**, 831 (1989).
[19] D.J. Werder, C.H. Chen, R.J. Cava, and B. Batlogg, Phys. Rev. B **38**, 5130 (1988).
[20] R. Beyers, B.T. Ahn, G. Gorman, V.Y. Lee, S.S.P. Parkin, M.L. Ramirez, K.P. Roche, J.E. Vazquez, T.M. Gür, and R.A. Huggins, Nature (London) **340**, 619 (1989).
[21] Th. Zeiske, D. Hohlwein, R. Sonntag, F. Kubanek, and Th. Wolf, Physica C **194**, 1 (1992).
[22] J. Grybos, D. Hohlwein, Th. Zeiske, R. Sonntag, F. Kubanek, K. Eichhorn, and Th. Wolf, Physica C **220**, 138 (1994).
[23] P. Burlet, V.P. Plakthy, C. Marin, and J.Y. Henry, Phys. Lett. A **167**, 401 (1992).
[24] Th. Zeiske, D. Hohlwein, R. Sonntag, J. Grybos, K. Eichhorn, and Th. Wolf, Physica C **207**, 333 (1993).
[25] D. Hohlwein, in *Materials and Crystallographic Aspects of HT_c-Superconductivity*, edited by E. Kaldis (Kluwer Academic, The Netherlands, 1994), p. 65.
[26] E. Straube, D. Hohlwein, and F. Kubanek, Physica C **295**, 1 (1998).
[27] W. Schwarz, O. Blaschko, G. Collin, and F. Marucco, Phys. Rev. B **48**, 6513 (1993).
[28] R.A. Hadfield, P. Schleger, H. Casalta, N.H. Andersen, H.F. Poulsen, M. von Zimmermann, J.R. Schneider, M.T. Hutchings, D.A. Keen, Ruixing Liang, P. Dosanjh, and W.N. Hardy, Physica C **235-240**, 1267 (1994).
[29] V. Plakhty, P. Burlet, and J.Y. Henry, Phys. Lett. A **198**, 256 (1995).
[30] E. Straube, D. Hohlwein, and F. Kubanek, Physica C **295**, 1 (1998).
[31] M.A. Alario-Franco, C. Chaillout, J.J. Capponi, J. Chenavas, and M. Marezio, Physica C **156**, 455 (1988).
[32] R. Sonntag, D. Hohlwein, T. Brückel, and G. Collin, Phys. Rev. Lett. **66**, 1497 (1991).
[33] T. Frello, N.H. Andersen, J. Madsen, A.B. Abrahamsen, M. von Zimmermann, T. Niemöller, J.R. Schneider, and Th. Wolf, Phys. Rev. B **61**, R9253 (2000).
[34] D. Mønster, P.-A. Lindgård, and N.H. Andersen, Phys. Rev. B **64**, 224520 (2001).
[35] R. Liang, P. Dosanjh, D.A. Bonn, D.J. Baar, J.F. Carolan, and W.N. Hardy, Physica C **195**, 51 (1992).
[36] N.H. Andersen, B. Lebech, and H.F. Poulsen, Physica C **172**, 31 (1990).
[37] P. Schleger, W. Hardy, and B. Yang, Physica C **176**, 261 (1991).
[38] H. Casalta, P. Schleger, P. Harris, B. Lebech, N.H. Andersen, R. Liang, P. Dosanjh, and W.N. Hardy, Physica C **258**, 321 (1996).
[39] R. Bouchard, D. Hupfeld, T. Lippmann, J. Neuefeind, H.-B. Neumann, H.F. Poulsen, U. Rütt, T. Schmidt, J.R. Schneider, J. Süssenbach, and M. von Zimmermann, Synchrotron Radiat. News **5**, 90 (1998).
[40] H.F. Poulsen, M. von Zimmermann, J.R. Schneider, N.H. Andersen, P. Schleger, J. Madsen, R. Hadfield, H. Casalta, R. Liang, P. Dosanjh, and W.N. Hardy, Phys. Rev. B **53**, 15 335 (1996).
[41] H.-B. Neumann, J.R. Schneider, J. Süssenbach, S.R. Stock, and Z.U. Rek, Nucl. Instrum. Methods Phys. Res. A **372**, 551 (1996).
[42] T. Fiig, N.H. Andersen, J. Berlin, and P.A. Lindgård, Phys. Rev. B **51**, 12 246 (1995).
[43] A.J. Bray, Adv. Phys. **43**, 357 (1994).
[44] V. Plakhty, A. Statilatov, Yu. Chernenkov, V. Fedorov, S.K. Sinha, Chun L. Loong, G. Gaulin, M. Vlasov, and S. Moshkin, Solid State Commun. **84**, 639 (1992).
[45] P. Schleger, H. Casalta, R. Hadfield, H.F. Poulsen, M. von Zimmermann, N.H. Andersen, J.R. Schneider, R. Liang, P. Dosanjh, and W.N. Hardy, Physica C **241**, 103 (1995).
[46] T. Schmidt, D. Woo, S. Keitel, J.R. Schneider, U. Lambert, and W. Zulehner, J. Appl. Crystallogr. **31**, 625 (1998).
[47] M.v. Zimmermann, J.R. Schneider, T. Frello, N.H. Andersen, J. Madsen, M. Käll, H. F. Poulsen, Th. Wolf, Ruixing Liang, P. Dosanjh, and W. N. Hardy (unpublished).
[48] R. Liang, D.A. Bonn, and W.N. Hardy, Physica C **336**, 57 (2000).
[49] C. Chillout, M.A. Alario-Franco, J.J. Capponi, J. Chenavas, J.L. Hodeau, and M. Marezio, Phys. Rev. B **36**, 7118 (1987).
[50] Th. Zeiske, D. Hohlwein, R. Sonntag, F. Kubanek, and G. Collin, Z. Phys. B: Condens. Matter **86**, 11 (1992).
[51] V. Plakhty, B. Kviatkovsky, A. Stratilatov, Yu. Chernenkov, P. Burlet, J.Y. Henry, C. Marin, E. Ressouche, J. Schweizer, F. Yakou, E. Elkaim, and J.P. Lauriat, Physica C **235-240**, 867 (1994).
[52] T. Fiig, N.H. Andersen, P.-A. Lindgård, J. Berlin, and O.G. Mouritsen, Phys. Rev. B **54**, 556 (1996).
[53] D. de Fontaine, L.T. Wille, and S.C. Moss, Phys. Rev. B **36**, 5709 (1987).
[54] P.A. Sterne and L.T. Wille, Physica C **162-164**, 223 (1989).
[55] A.G. Khachaturyan and J.W. Morris, Phys. Rev. Lett. **64**, 76 (1990).
[56] A. Bertinotti, J. Hammann, D. Luzet, and A. Vinzent, Physica C **160**, 227 (1989).
[57] F. Yakhou, V. Plakhty, A. Stratilatov, P. Burlet, J.P. Lauriat, E. Elkaim, J.Y. Henry, M. Vlasov, and S. Moshkin, Physica C **261**, 315 (1996).
[58] T. Krekels, T.S. Shi, J. Reyes-Gasga, G. van Tendeloo, J. van Landuyt, and S. Amelinckx, Physica C **167**, 677 (1990).

[59] T. Krekels, S. Kaesche, and G. van Tendeloo, Physica C **248**, 317 (1995).

[60] D.J. Werder, C.H. Chen, and G.P. Espinosa, Physica C **173**, 285 (1991).

[61] H. Tolentino, F. Baudelet, A. Fontaine, T. Gourieux, G. Krill, J.Y. Henry, and J. Rossat-Mignod, Physica C **192**, 115 (1992).

[62] H. Lüetgemeier, S. Schmenn, P. Meuffels, O. Storz, R. Schölhorn, Ch. Niedermeier, I. Heinmaa, and Yu. Baikov, Physica C **267**, 191 (1996).

[63] A.A. Aligia, J. Garcés, and H. Bonadeo, Phys. Rev. B **42**, 10 226 (1990).

[64] A.A. Aligia, J. Garcés, and J.P. Abriata, Physica C **221**, 109 (1994).